

Article

Dispersion of Elastic Waves in Functionally Graded CNTs-Reinforced Composite Beams

Ali Seyfi¹, Amir Teimouri¹, Rossana Dimitri²  and Francesco Tornabene^{2,*} 

¹ Department of Mechanical Engineering, Amirkabir University of Technology, Hafez Ave, Tehran 15875, Iran; aliseyfi@aut.ac.ir (A.S.); ateimouri@aut.ac.ir (A.T.)

² Department of Innovation Engineering, University of Salento, 73100 Lecce, Italy; rossana.dimitri@unisalento.it

* Correspondence: francesco.tornabene@unisalento.it

Abstract: This work deals with the wave propagation analysis in functionally graded carbon nanotubes (CNTs)-reinforced composite beams lying on an elastic medium. Despite the large amount of experimental and theoretical studies in the literature on the mechanical behavior of composite structures strengthened with CNTs, limited attention has been paid to the effect of an axial graduation of the reinforcing phase on the mechanical response of CNTs-reinforced composite beams. In this paper, CNT fibers are graded across the beam length, according to a power-law function, which expresses a general variation from a linear to parabolic pattern. An Euler-Bernoulli beam theory is considered herein to model the CNTs-reinforced composite structure resting on a Winkler–Pasternak foundation, whose governing equations are derived from the Hamiltonian principle. The theoretical solution of the problem checks for the sensitivity of the mechanical response to different parameters, i.e., the wave number, power index, Winkler and Pasternak coefficients, that could serve for further computational/experimental studies on the same problem, even from a design standpoint.

Keywords: axially CNT-reinforced; composite beam; elastic foundation; Euler-Bernoulli beam theory; wave dispersion analysis



Citation: Seyfi, A.; Teimouri, A.; Dimitri, R.; Tornabene, F. Dispersion of Elastic Waves in Functionally Graded CNTs-Reinforced Composite Beams. *Appl. Sci.* **2022**, *12*, 3852. <https://doi.org/10.3390/app12083852>

Academic Editor: Fuji Wang

Received: 27 February 2022

Accepted: 6 April 2022

Published: 11 April 2022

Publisher's Note: MDPI stays neutral with regard to jurisdictional claims in published maps and institutional affiliations.



Copyright: © 2022 by the authors. Licensee MDPI, Basel, Switzerland. This article is an open access article distributed under the terms and conditions of the Creative Commons Attribution (CC BY) license (<https://creativecommons.org/licenses/by/4.0/>).

1. Introduction

The performance of structures mainly depends on their constitutive materials whose proper selection represents one of the most challenging subjects in manufacturing processes. Accordingly, engineers and researchers have performed great efforts to find and use composite materials with optimal physical and chemical properties, depending on their structural applications in marine, automotive and building constructions [1–5]. To obtain a performing structure in terms of dynamic behavior, the use of laminates and composite materials is widely proposed in many contexts. This kind of technical solution, indeed, can tailor the local and global stiffness as well as the weight of structures according to a desired loading and design demand. In the last years, a novel class of reinforced composite materials relies on carbon-based materials, where CNTs, graphene, graphene platelets (GPLs), and graphene oxide, represent outstanding possibilities of reinforcement with even, uneven, and/or functionally graded distributions within the matrix [6,7].

In such a context, different studies on composites/nanocomposites have been performed by researchers, even focusing on hybrid nanocomposites reinforced by a combination of fillers, such as GPLs, CNTs, and carbon fibers (CFs) within the matrix [8–10]. Among different problems, the dynamic behavior of composite structures represents a key aspect for a proper selection of the reinforcement phase during a design process. More specifically, due to the large use of composite materials in structural members with different geometries, several higher-order formulations have been proposed in the literature to study their linear and/or nonlinear behavior, including vibration and buckling problems. Except for classical plate theories (CPTs), higher-order shear deformation theories (HSDT) are

more appropriate for studying complicated geometries, especially for structural elements with increased thicknesses. Among the recent literature, Han et al. [11] used a hybrid analytical/two-dimensional finite element method (FEM) to solve the wave propagation problem of fluid-conveying composite pipes. In addition, Ghadiri et al. [12] analyzed the influence of a non-ideal support on the vibrational behavior of laminated composite classic beams carrying a mass-spring-damper system subjected to an axial force; Amabili [13] applied a third-order shear deformation theory (TSDT) to explore geometrically the nonlinear bending and vibration analysis of laminated doubly curved shells. Among coupled problems, Nguyen et al. [14] explored the dynamic and buckling properties of laminated composite beams exposed to thermomechanical loading in the framework of HSDTs.

Heydarpour et al. [15] studied the free vibrational behavior of CNT-reinforced composite truncated conical shells considering the effect of centrifugal and Coriolis forces based on an FSDT. Similarly, Zhang et al. [16] used the FSDT and element-free IMLS-Ritz method to solve the dynamic problem of functionally graded CNT-reinforced composite (FG-CNTRC) triangular plates; the same FSDT-based approach was applied by García-Macías et al. [17] to study the bending and dynamic behavior of thin and moderately thick FG-CNTRC skew plates with uniaxially aligned reinforcements. A post-buckling analysis of FG-CNTRC beams in thermal environment was performed by Wu et al. [18] always based on an FSDT. The same basics were also applied in Refs. [19–21] to investigate the frequency response of elliptical plates made of FG-CNTRC, the dynamics of FG-CNTRC beams under arbitrary boundary conditions, and the effect of thermal loading on the vibrational response of temperature-dependent FG-CNTRC cylindrical porous shells with the help of a generalized differential quadrature method (GDQM).

In the last years, Ebrahimi et al. [22–24] examined the effect of the reinforcement agglomeration on the wave propagation in multiscale hybrid nanocomposite beams, plates, and shells. Additionally, Qaderi et al. [25] studied the free dynamic properties of GPLs-reinforced sandwich composite beams lying on a viscoelastic medium based on HSDTs; whereas Ebrahimi et al. [26] analyzed the dispersion of waves in GPLs-reinforced composite porous shells based on a FSDT. Furthermore, Javani et al. [27] probed thermal buckling of GPLs-reinforced composite annular plates based upon FSDT and GDQM. The same computational approach has been applied, recently, in [28] to analyze the axially FG-CNTRC beams lying on an elastic medium. A similar analysis can be also found in [29] to examine the thermal post-buckling response of FG-CNTRC curved panels lying on an elastic substrate with elastic restrained edges. Ebrahimi et al. [30] applied a refined HSDT to study the wave dispersion characteristics of plates reinforced with graphene oxide powder immersed in a thermal environment. Among nonlocal formulations, a nonlocal strain gradient theory was implemented by Merzouki et al. [31] to solve the bending problem of porous GPL-strengthened nanocomposite beams based on finite elements. A nonlinear frequency analysis of thin-walled CNTRC shells was also performed recently by Mahmure et al. [32], accounting for the effect of an elastic medium; whereas Ebrahimi and Seyfi [33] studied the effect of agglomeration and waviness factors of nano-reinforcements on the wave propagation behavior of embedded nanocomposite beams strengthened with multi-walled carbon nanotubes, as provided by HSDTs.

Despite the large literature on the topic, to date, there is a general lack of works analyzing the wave propagation of longitudinally CNTs-reinforced composite beams lying on an elastic medium. A complete investigation about the problem, indeed, should include different environmental, loading, and boundary conditions. In the last case, we have to account for the possible interaction between a structural component and the surrounding elastic medium or foundation, whose properties can vary linearly and/or nonlinearly.

This aspect is analyzed herein from a theoretical perspective for CNTs-reinforced composite beams resting on elastic media. The CNTs distribution is modeled according to a power-law function that can embrace from linear to parabolic reinforcement patterns. A numerical investigation is repeated systematically to check for the influence of various input parameters (i.e., wave number, power index, foundation parameters) on

the overall response that could serve as benchmarks for design purposes and further computational/experimental analyses on the same problem.

2. Theory and Formulation

2.1. CNTs-Reinforced Composite Structures

Various methods of mixtures can be employed to define the main mechanical properties of composite structures such as plates, beams and shells reinforced with CNTs. According to such homogenization techniques, the volume fraction of CNTs plays a key role in the variation of mechanical properties of composite structures. For CNT-reinforced on dimensional structures, the equivalent material properties read as [20]

$$E(x) = E_m V_m(x) + e_1 E_{11,CNT} V_{CNT}(x) \tag{1}$$

$$\nu(x) = \nu_{CNT} V_{CNT}(x) + \nu_m V_m(x) \tag{2}$$

$$\rho(x) = \rho_{CNT} V_{CNT}(x) + \rho_m V_m(x) \tag{3}$$

where E , ν , and ρ denote the Young’s modulus, Poisson’s ratio, and density, respectively, e_1 is a coefficient, which refers to the manufacturing efficiency of the CNT-matrix mixture. In addition, x refers to the arbitrary coordinate between 0 and L , subscripts m and CNT stand for properties related to the CNT matrix and fibers, respectively. This means that V_{CNT} and V_m is the volume fraction of CNTs and matrix, respectively, which satisfy the following laws [34]

$$V_{CNT}(x) = \left(1 - \frac{x}{L}\right)^k V_{CNT-L} - \left(\left(1 - \frac{x}{L}\right)^k - 1\right) V_{CNT-R} \tag{4}$$

$$V_m(x) = 1 - V_{CNT}(x) \tag{5}$$

k being a power term. Moreover, V_{CNT-R} and V_{CNT-L} represents the volume fraction of CNT fibers on the right and the left sides of the structure, respectively. The total volume fraction of the CNT fibers in the whole structure is expressed in the following form

$$V_{CNT-Total} = \frac{V_{CNT-L} + k V_{CNT-R}}{k + 1} \tag{6}$$

Note that the CNTs volume fraction at the left side of the beam can be obtained using $k = 0$ in the last relation.

2.2. Problem Description and Fundamental Equations

The structural model relies on the following constitutive relations [35]

$$\{\sigma\} = [Q]\{\varepsilon\} \tag{7}$$

where $Q_{ij} = Q_{ij}(x)$, $i, j = 1, \dots, 6$ stands for the stiffness properties, and $\{\sigma\}^T = \{\sigma_{xx} \ \sigma_{yy} \ \sigma_{zz} \ \sigma_{xy} \ \sigma_{xz} \ \sigma_{yz}\}^T$, $\{\varepsilon\}^T = \{\varepsilon_{xx} \ \varepsilon_{yy} \ \varepsilon_{zz} \ \varepsilon_{xy} \ \varepsilon_{xz} \ \varepsilon_{yz}\}^T$ refer to the stress and strain vector, respectively. For orthotropic structures, the constitutive relations read as follows [36]

$$\begin{Bmatrix} \sigma_{xx} \\ \sigma_{yy} \\ \sigma_{zz} \\ \sigma_{xy} \\ \sigma_{xz} \\ \sigma_{yz} \end{Bmatrix} = \begin{bmatrix} Q_{11} & Q_{12} & Q_{13} & 0 & 0 & 0 \\ Q_{21} & Q_{22} & Q_{23} & 0 & 0 & 0 \\ Q_{31} & Q_{32} & Q_{33} & 0 & 0 & 0 \\ 0 & 0 & 0 & Q_{44} & 0 & 0 \\ 0 & 0 & 0 & 0 & Q_{55} & 0 \\ 0 & 0 & 0 & 0 & 0 & Q_{66} \end{bmatrix} \begin{Bmatrix} \varepsilon_{xx} \\ \varepsilon_{yy} \\ \varepsilon_{zz} \\ \varepsilon_{xy} \\ \varepsilon_{xz} \\ \varepsilon_{yz} \end{Bmatrix} \tag{8}$$

Based on a classic Euler-Bernoulli beam theory, the displacement field for a CNTs-strengthened composite beam is defined as

$$u_1 = \eta(x, t) - z \frac{\partial \zeta(x, t)}{\partial x} \tag{9}$$

$$u_2 = \zeta(x, t) \tag{10}$$

accounting for the displacement components of the mid-plane of the beam in the length and thickness directions, η and ζ , respectively. The nonzero strain component of the composite beam reads as follows

$$\epsilon_{xx} = \frac{\partial \eta(x, t)}{\partial x} - z \frac{\partial^2 \zeta(x, t)}{\partial x^2} \tag{11}$$

Hereafter, we consider a beam embedded on an elastic medium, as depicted in Figure 1, accounting for a Pasternak coefficient, K_P , as a shear layer and a Winkler coefficient, K_W , as normal layer. The elastic foundation is generally defined by using the stiffness coefficient and power-law distribution function as [37].

$$K_P(x) = K_{P0} \left(1 - \beta \left(\frac{x}{L} \right)^m \right) \tag{12}$$

$$K_W(x) = K_{W0} \left(1 - \alpha \left(\frac{x}{L} \right)^n \right) \tag{13}$$

depending on the power term n and coefficient α . Moreover, K_{W0} stands for the initial value of the Winkler coefficient, whereas the Pasternak coefficient is likewise demonstrated using an initial value, power term, and coefficient of K_{P0} , m , and β , respectively.

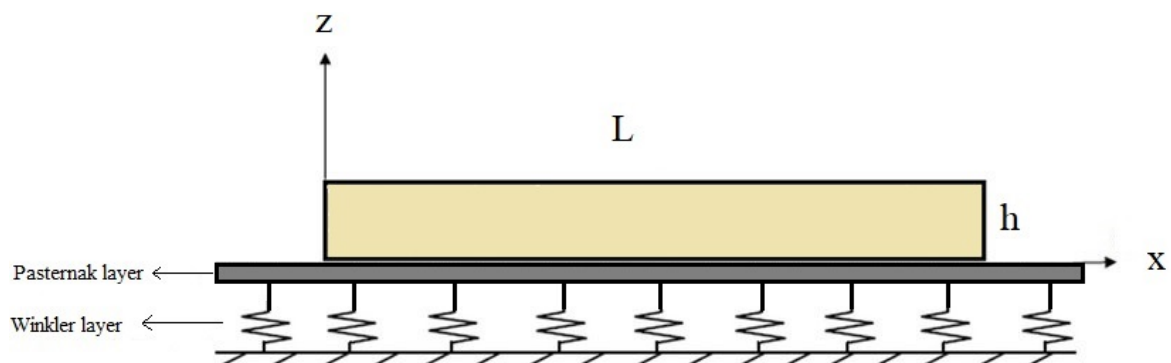


Figure 1. Geometrical model of composite beam on a Winkler-Pasternak foundation.

The equations of motion for the CNTs-reinforced structure are determined based on the Hamiltonian principle, i.e.,

$$\int_{t_0}^{t_1} \delta(\Phi + W_{nc} - T) dt = 0 \tag{14}$$

where Φ refers to the strain energy, T is the kinetic energy, W_{nc} is the work done by non-conservative external forces, and t is the time variable. Each energy quantity can be defined in variational form as

$$\delta \Phi = \frac{1}{2} \int_A \int_0^L \sigma_{xx} \delta \epsilon_{xx} dx dA = \frac{1}{2} \int_A \int_0^L \sigma_{xx} \left(\delta \frac{\partial \eta(x, t)}{\partial x} - z \delta \frac{\partial^2 \zeta(x, t)}{\partial x^2} \right) dx dA \tag{15}$$

$$\delta T = \frac{1}{2} \int_0^L \int_A \rho(x) \delta \left(\left(\frac{\partial \eta(x, t)}{\partial t} - z \frac{\partial^2 \zeta(x, t)}{\partial x \partial t} \right)^2 + \left(\frac{\partial \zeta(x, t)}{\partial t} \right)^2 \right) dA dx \tag{16}$$

$$\delta W_{nc} = \frac{1}{2} \int_0^L \delta \left(K_W(x) \zeta^2(x, t) + K_P(x) \left(\frac{\partial \zeta(x, t)}{\partial x} \right)^2 \right) dx \tag{17}$$

which are substituted in the Hamiltonian principle (14) to yield the following equations of motion

$$\delta u \rightarrow \frac{\partial}{\partial x} \left(B(x) \frac{\partial^2 \zeta}{\partial x^2} - A(x) \frac{\partial \eta(x, t)}{\partial x} \right) - I_1(x) \frac{\partial^3 \zeta(x, t)}{\partial x \partial t^2} + I_0(x) \frac{\partial \eta^2(x, t)}{\partial t^2} = 0 \tag{18}$$

$$\begin{aligned} \delta w \rightarrow & \frac{\partial}{\partial x} \left(I_1(x) \frac{\partial^2 \eta(x, t)}{\partial t^2} - I_2(x) \frac{\partial^3 \zeta(x, t)}{\partial x \partial t^2} - K_P(x) \frac{\partial \zeta(x, t)}{\partial x} \right) + \\ & + \frac{\partial^2}{\partial x^2} \left(D(x) \frac{\partial^2 \zeta(x, t)}{\partial x^2} - B(x) \frac{\partial \eta(x, t)}{\partial x} \right) + K_W(x) \zeta(x, t) + I_0(x) \frac{\partial^2 \zeta(x, t)}{\partial t^2} = 0 \end{aligned} \tag{19}$$

Along with the following boundary conditions

$$A(x) \frac{\partial \eta(x, t)}{\partial x} \delta \eta(x, t) \Big|_{x=0}^{x=L} - B(x) \frac{\partial^2 \zeta(x, t)}{\partial x^2} \delta \eta(x, t) \Big|_{x=0}^{x=L} = 0 \tag{20}$$

$$\frac{\partial}{\partial x} \left(B(x) \frac{\partial \eta(x, t)}{\partial x} \right) \delta \zeta(x, t) \Big|_{x=0}^{x=L} - \frac{\partial}{\partial x} \left(D(x) \frac{\partial^2 \zeta(x, t)}{\partial x^2} \right) \delta \zeta(x, t) \Big|_{x=0}^{x=L} = 0 \tag{21}$$

$$B(x) \frac{\partial \eta(x, t)}{\partial x} \delta \left(\frac{\partial \zeta(x, t)}{\partial x} \right) \Big|_{x=0}^{x=L} - D(x) \frac{\partial^2 \zeta(x, t)}{\partial x^2} \delta \left(\frac{\partial \zeta(x, t)}{\partial x} \right) \Big|_{x=0}^{x=L} = 0 \tag{22}$$

For symmetry reasons throughout the thickness, the inertial terms I_0, I_1, I_2 become as follows

$$\begin{Bmatrix} I_0(x) \\ I_2(x) \end{Bmatrix} = (\rho_m + (\rho_{CNT} - \rho_m) V_{CNT}(x)) \begin{Bmatrix} A \\ I \end{Bmatrix}, I_1 = 0 \tag{23}$$

The stiffness terms A, D and B are determined as

$$\begin{Bmatrix} A(x) \\ D(x) \end{Bmatrix} = \int_{-h/2}^{h/2} \left(\frac{E_m + (e_1 E_{11,CNT} - E_m) V_{CNT}(x)}{1 - \nu^2(x)} \right) \begin{Bmatrix} 1 \\ z^2 \end{Bmatrix} dz, B(x) = 0 \tag{24}$$

After a brief mathematical manipulation, the equations of motion and boundary conditions take the following form

$$I_0(x) \frac{\partial^2 \zeta(x, t)}{\partial t^2} + K_W(x) \zeta(x, t) - \frac{\partial}{\partial x} \left(I_2(x) \frac{\partial^3 \zeta(x, t)}{\partial x \partial t^2} + K_P(x) \frac{\partial \zeta(x, t)}{\partial x} - \frac{\partial D(x)}{\partial x} \frac{\partial^3 \zeta(x, t)}{\partial x^3} \right) = 0 \tag{25}$$

$$I_0(x) \frac{\partial \eta^2(x, t)}{\partial t^2} - \frac{\partial}{\partial x} \left(A(x) \frac{\partial \eta(x, t)}{\partial x} \right) = 0 \tag{26}$$

$$\tilde{V} = (V_{CNT-L} - V_{CNT-R})(k)(1 - x)^{(k)} \tag{27}$$

By substituting Equations (18) and (19) into Equations (20) and (21) and using Equations (4), (5), (11) and (27), the governing equations of the problem become as follows

$$\begin{aligned} & \left(\left(1 - \left(1 - e_1 \frac{E_{11,CNT}}{E_m} \right) \left(\frac{\tilde{V}}{k} + V_{CNT-R} \right) \right) \frac{\partial^2 \eta(x, t)}{\partial x^2} + \left(1 - e_1 \frac{E_{11,CNT}}{E_m} \right) \frac{\tilde{V}}{1-x} \frac{\partial \eta(x, t)}{\partial x} \right) \frac{1}{\gamma^2(1-\nu^2)} + \\ & + \left(\left(1 - \frac{\rho_{CNT}}{\rho_m} \right) V_{CNT}(x) - 1 \right) \frac{\partial \eta^2(x, t)}{\partial t^2} = 0 \end{aligned} \tag{28}$$

$$\begin{aligned} & - \left(1 + \left(\frac{\rho_{CNT}}{\rho_m} - 1 \right) \left(\frac{\tilde{V}}{k} + V_{CNT-R} \right) \right) \frac{\partial^2 \zeta(x, t)}{\partial t^2} + \left(1 + \left(\frac{\rho_{CNT}}{\rho_m} - 1 \right) \left(\frac{\tilde{V}}{k} + V_{CNT-R} \right) \right) \gamma^2 \frac{\partial^4 \zeta(x, t)}{\partial x^2 \partial t^2} + \\ & - \left(1 - \frac{\rho_{CNT}}{\rho_m} \right) \frac{\tilde{V}}{1-x} \gamma^2 \frac{\partial^3 \zeta(x, t)}{\partial x \partial t^2} - \left(\left(1 + \left(e_1 \frac{E_{11,CNT}}{E_m} - 1 \right) \left(\frac{\tilde{V}}{k} + V_{CNT-R} \right) \right) \frac{\partial^4 \zeta(x, t)}{\partial x^4} + \right. \\ & + 2 \left(1 - e_1 \frac{E_{11,CNT}}{E_m} \right) \frac{\tilde{V}}{1-x} \frac{\partial^3 \zeta(x, t)}{\partial x^3} + \left. \left(e_1 \frac{E_{11,CNT}}{E_m} - 1 \right) \frac{(k-1) \tilde{V}}{(1-x)^2} \frac{\partial^2 \zeta(x, t)}{\partial x^2} \right) \frac{1}{1-\nu^2} + \\ & - \left(m \beta x^{m-1} \frac{\partial \zeta(x, t)}{\partial x} + K_{W0}(1 - \alpha x^n) \zeta(x, t) \right) + K_{P0}(1 - \beta x^m) \frac{\partial^2 \zeta(x, t)}{\partial x^2} = 0 \end{aligned} \tag{29}$$

in which $\gamma = \sqrt{I/(AL^2)}$.

3. Solution Procedure

An analytical method is now implemented to solve the governing Equations (28) and (29), based on the following kinematic definition

$$u = Ue^{i(\beta_x x - \omega_n t)} \quad (30)$$

$$w = We^{i(\beta_x x - \omega_n t)} \quad (31)$$

in which U and W denote the wave amplitudes, β_x and ω_n denote the wave number and circular frequency propagated waves, respectively. By substitution of w and u from Equations (30) and (31) into Equations (28) and (29) we get the following eigenvalue problem

$$\left(\begin{bmatrix} k_{11} & k_{12} \\ k_{21} & k_{22} \end{bmatrix} - \omega_n^2 \begin{bmatrix} m_{11} & m_{12} \\ m_{21} & m_{22} \end{bmatrix} \right) \begin{bmatrix} U \\ W \end{bmatrix} = 0 \quad (32)$$

which is solved in terms of ω_n , and wave frequency. This means that the following determinant must be equal to zero

$$\left| \begin{bmatrix} K - \omega_n^2 M \end{bmatrix}_{2 \times 2} \right| = 0 \quad (33)$$

where the wave frequency f is defined as

$$f = \frac{\omega_n}{2\pi} \quad (34)$$

Thus, the phase velocity associated with the problem can be determined as

$$C = \frac{\omega_n}{\beta_x} \quad (35)$$

4. Numerical Results

In this section, we study the sensitivity of the wave frequency and phase velocity to different input parameters that could serve for design purposes of many high-tech devices made of advanced CNT-reinforced composite materials, and further computational studies on the topic. We start the analysis by accounting for the mechanical properties of the constituent materials in Table 1 for FG CNTs-reinforced composites, while validating the proposed methodology with findings by Loy [38] from literature. Table 2 summarizes the results in terms of dimensionless natural frequency for a simply-supported structure and different wave numbers, with a good correspondence between results based on our model and those once from literature. One of the critical aspects for such structures, relies on the influence of the CNT distribution in the length direction. To this end, we plot the wave frequency vs. the wave number for various CNTs volume fractions, while keeping fixed $K_{P0} = 10$ and $K_{W0} = 200$, as visible in Figure 2. For low wave numbers, up to the unit value, any variation in the wave frequency is noticed, after which a monotonic increase of wave frequency occurs for increased values of wave number. This behavior is even more pronounced for an increased volume fraction of the reinforcing phase. For a constant wave number, indeed, an increased volume fraction of CNTs gets higher values of wave frequency. A further investigation accounts for the influence of the volume fraction of CNTs and wave number on the phase velocity of the structure, as plotted in Figure 3. Note that for small wave numbers up to 0.1, the volume fraction does not affect the phase velocity, with a meaningful variation in the response for higher wave numbers in a non monotonic sense, both in the ascending and descending branches of the plots. Small variations in the volume fraction of CNTs within the range 0.1 and 10, enable a severe additive effect on the phase velocity, where the structure gets stiffer.

Table 1. Material properties of functionally graded CNTs-reinforced composite beam.

Properties	Units	CNT [28]	Matrix [28]
E	GPa	5646.6	2.5
ρ	Kg/m ³	1400	1190
ν	-	0.28	0.3

Table 2. Comparative evaluation of the dimensionless natural frequency. $\Omega = \omega R \sqrt{(1 - \nu^2)\rho/E}$ for a simply-supported isotropic shell and different wave numbers.

n	Loy [38]	Present
1	0.016102	0.0161011
2	0.009387	0.0093865
3	0.022108	0.0221045
4	0.042096	0.0420954
5	0.068008	0.0680080
6	0.099730	0.0997300

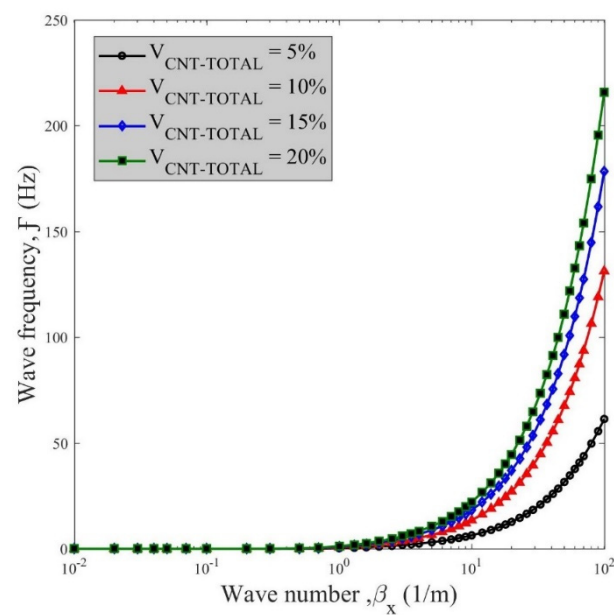


Figure 2. Wave frequency vs. wave number for various volume fractions of CNTs.

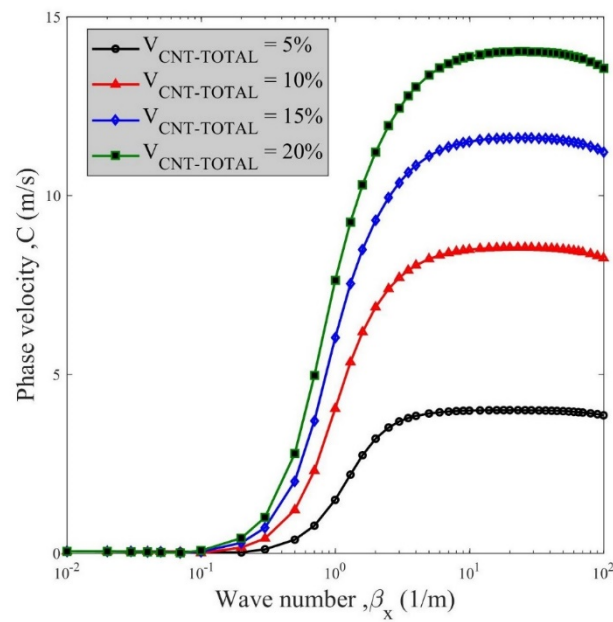


Figure 3. Phase velocity vs. wave number for various volume fractions of CNTs.

Figures 4 and 5 describe the variation of wave frequency and phase velocity versus the wave number for different CNT grading power terms at a fixed $V_{CNT-TOTAL} = 20\%$. Based on these plots, for high wave numbers, the influence of the power term is much more significant, where the power term plays a decreasing role in the variation of wave frequency. In both figures, the wave frequency and phase variation decrease for an increased power term, and a fixed wave number, due to a softening influence of the power term along with an overall increase in the structural deformability.

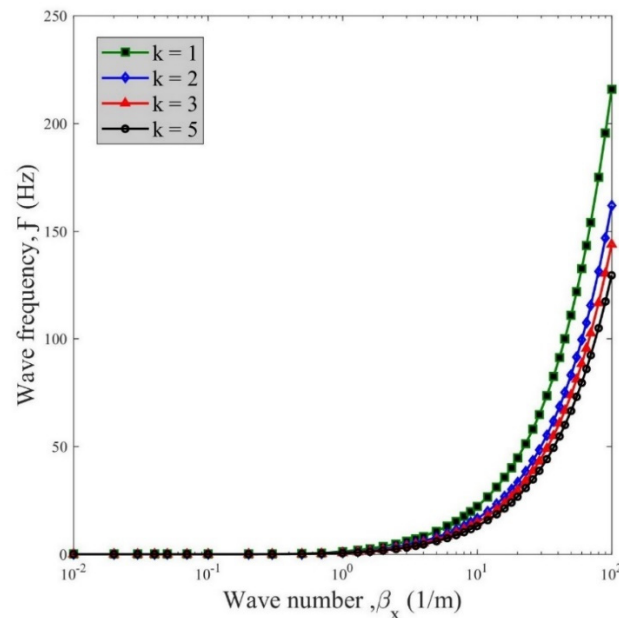


Figure 4. Wave frequency vs. wave number for different values of k .

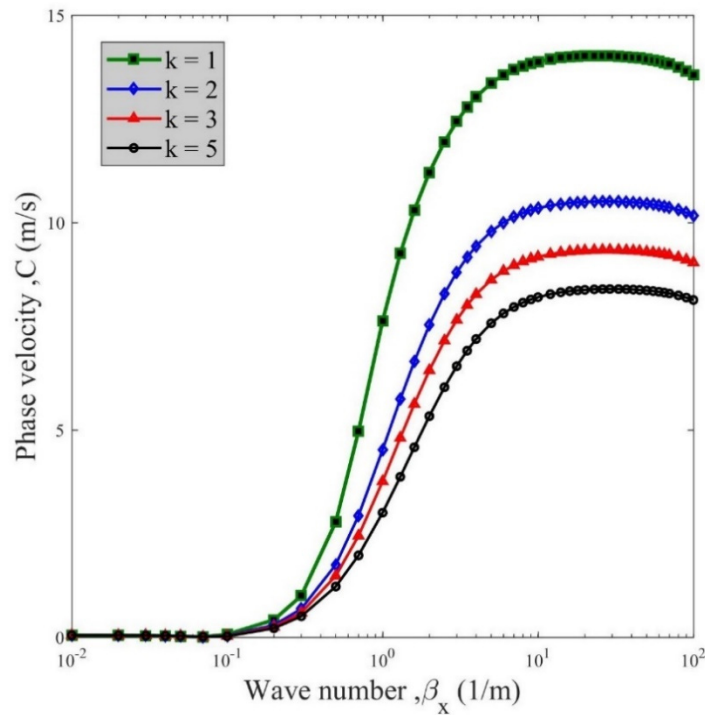


Figure 5. Phase velocity vs. wave number for different values of k .

Figure 6 also shows the effect of the Winkler coefficient on the wave frequency for a different coefficient α , here varied from 0.2 to 0.8, under the assumption $V_{CNT-L} = 5\%$, $K_{P0} = 10$. When the structure is supported by a foundation, the structural stiffness increases monotonically with K_W , since the wave frequency gets higher values for an increased Winkler coefficient, especially for lower values of the coefficient α . Another important parameter for structures on an elastic foundation is represented by the Pasternak coefficient in the shear layer. Figure 7 shows the influence of this parameter on the phase velocity, while varying the coefficient β from 0.2 up to 0.8. It is worth noticing that an increased Pasternak coefficient yields higher phase velocities for each selected β , whereas the phase velocity becomes smaller by increasing the coefficient β from 0.2 up to 0.8 under the same Pasternak coefficient assumption.

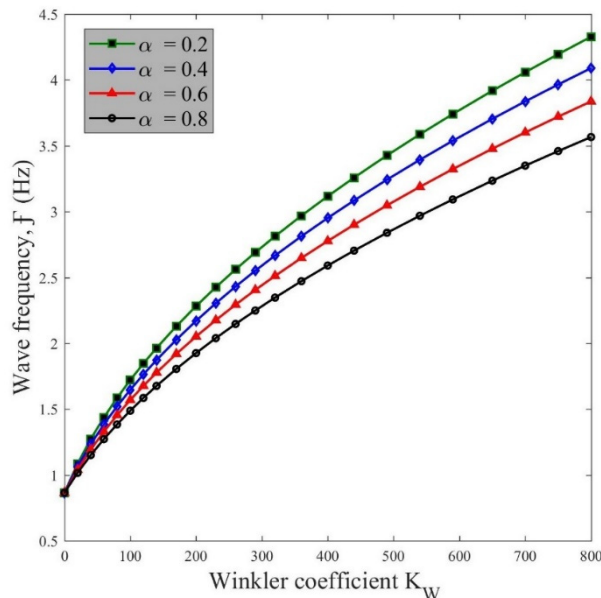


Figure 6. Wave frequency vs. Winkler parameter for various α .

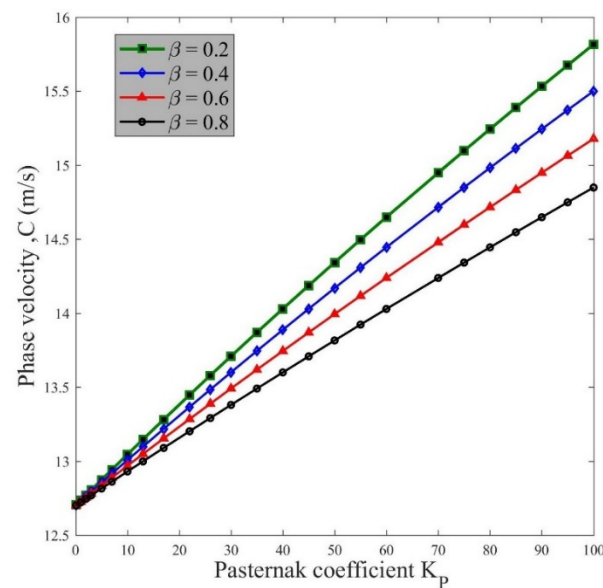


Figure 7. Phase velocity vs. Pasternak parameter for different β .

In Figure 8 we plot the influence of the Winkler coefficient on the wave frequency for different power terms n , with a monotonic hardening effect of the Winkler coefficient on the structural response, especially for increased values of n . It is clearly evident that the wave frequency increases for an increased power term n , and a fixed Winkler coefficient K_W , while increasing monotonically with K_W under the same assumption of n . Similar observations can be repeated for a varying Pasternak foundation coefficient and power term m (see Figure 9) whose response sensitivity is more accentuated for different values of m , compared to that one stemming from a Winkler foundation. A further parametric investigation accounts for the variation of the wave frequency with the rational volume fraction at the right and left side of the structure (V_{CNT-R}/V_{CNT-L}) for various power terms k . As plotted in Figure 10, such rational value V_{CNT-R}/V_{CNT-L} can affect significantly the wave frequency of the structure, especially for increased values of k , with an overall hardening effect for increased values of V_{CNT-R}/V_{CNT-L} and fixed power term k . Such effect is also observed for an increased value of k from one to five, while keeping fixed the rational value V_{CNT-R}/V_{CNT-L} . The last two parametric investigations account for the sensitivity of the structural wave frequency (Figure 11) and phase velocity (Figure 12) for different volume fractions (in percentage) of CNTs on the left side of the beam, and different CNTs power terms. Based on both figures, an increased volume fraction of CNTs as reinforcing phase within the material makes the structure stiffer, as visible from the increased wave frequency and phase velocity. Both values get higher for an increased power term k , especially for higher volume fractions of CNTs.

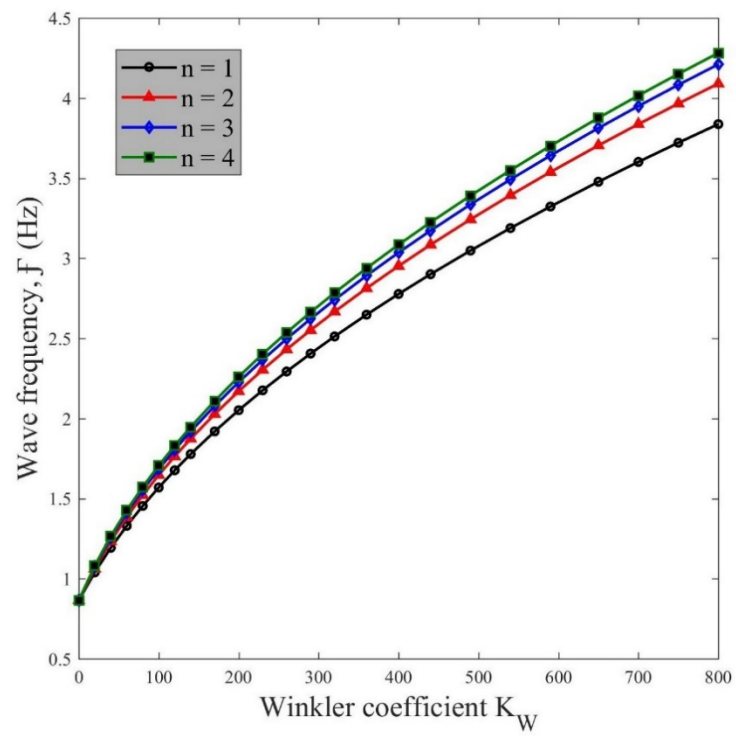


Figure 8. Wave frequency vs. Winkler parameter for various n .

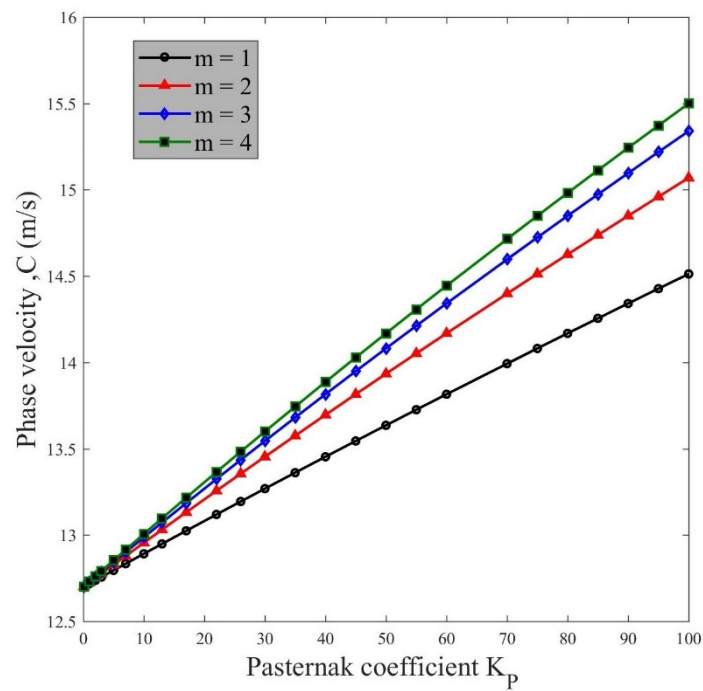


Figure 9. Phase velocity vs. Pasternak parameter for different m .

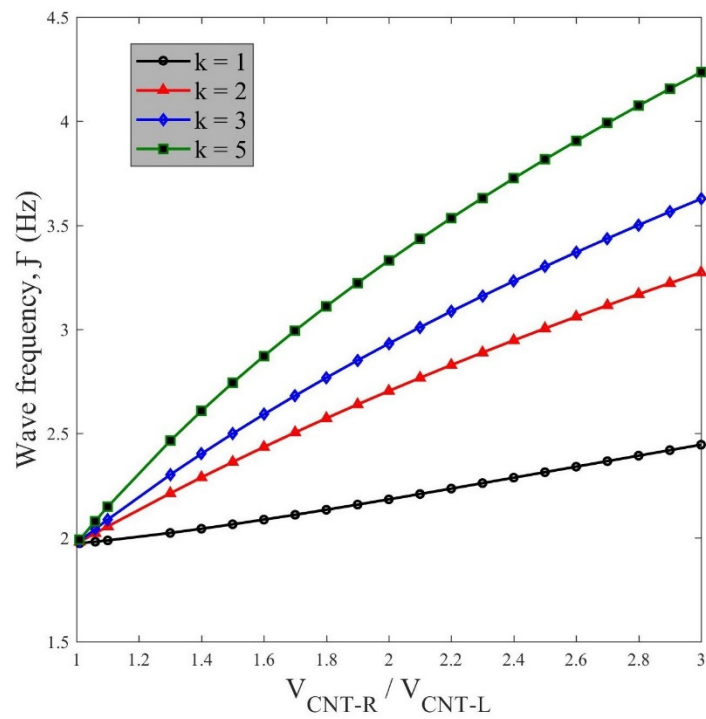


Figure 10. Wave frequency vs. the rational value V_{CNT-R} / V_{CNT-L} for different k .

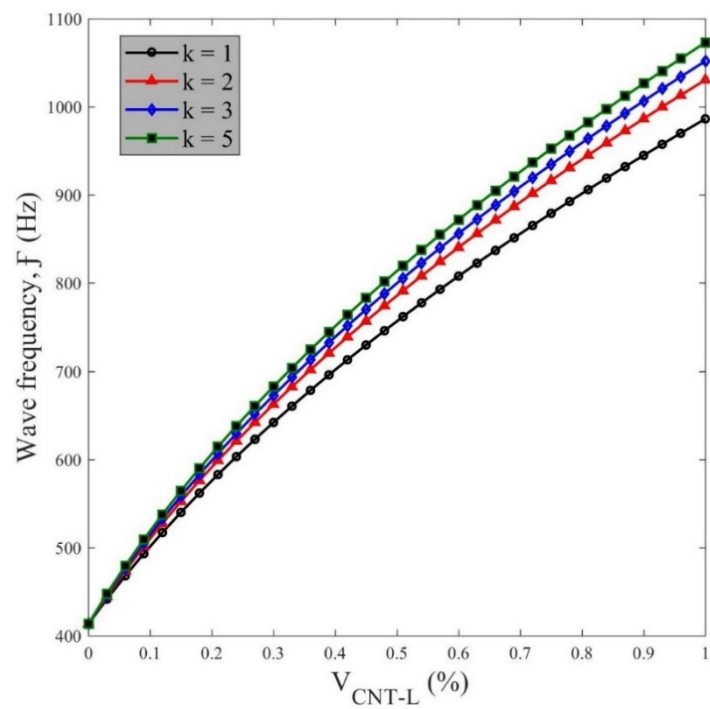


Figure 11. Wave frequency vs. V_{CNT-L} for various k .

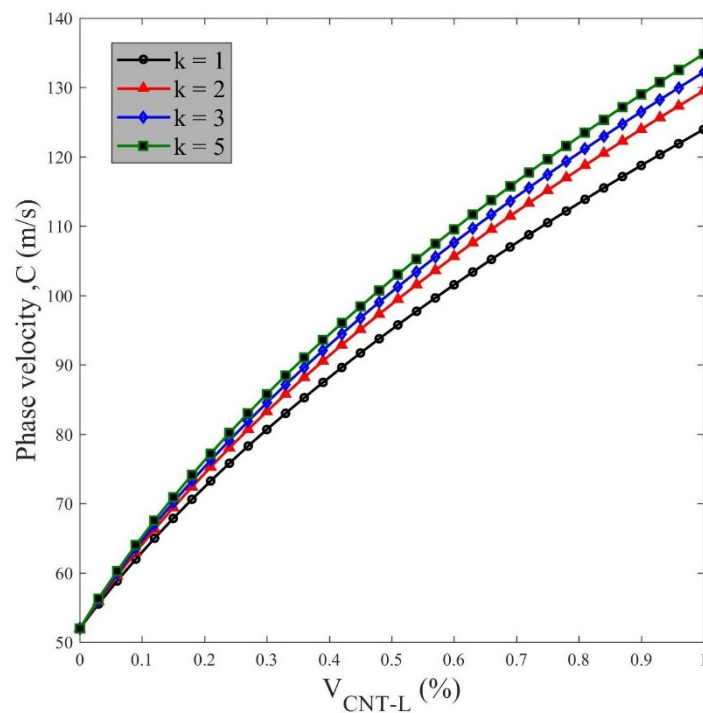


Figure 12. Phase velocity vs. V_{CNT-L} for different k .

5. Conclusions

The present work deals with the wave dispersion in longitudinally FG CNTs-reinforced composite beams lying on an elastic medium, modeled as a Winkler–Pasternak foundation. The gradation of CNT fibers is here modeled by means of a power-law function, defining a variation from linear to parabolic distributions. The equations of motion of the composite beams rely on a classic Euler–Bernoulli beam theory and Hamiltonian principle, whose theoretical results can be summarized as follows:

- The phase velocity and wave frequency of the composite beam can be improved by increasing the volume fraction of CNT fibers and the power term k .
- The Winkler–Pasternak foundation affects significantly the wave propagation response of composite beam structures. The enhancement of Winkler and Pasternak coefficients has a beneficial effect on the phase velocity and wave frequency, whose increased values can be related to an improved overall stiffness of the structure. The wave frequency and phase velocity reduce significantly by selecting higher values of coefficient α within the power law distribution function.
- The CNTs volume fraction at both sides of the beam, has a meaningful influence on the wave propagation. The volume fraction at the left side of the beam (V_{CNT-L}) and the V_{CNT-R}/V_{CNT-L} ratio has a hardening effect on the structure, with an improved response in terms of wave frequency and phase velocity.

Author Contributions: Conceptualization, R.D. and F.T.; Data curation, R.D. and F.T.; Formal analysis, A.S., A.T., R.D. and F.T.; Investigation, A.S., A.T., R.D. and F.T.; Methodology, R.D. and F.T.; Software, F.T.; Supervision, R.D. and F.T.; Validation, R.D. and F.T.; Writing—Original draft, A.S. and A.T.; Writing—Review & editing, R.D. and F.T. All authors have read and agreed to the published version of the manuscript.

Funding: This research received no external funding.

Conflicts of Interest: The authors declare no conflict of interest.

References

1. Mal, A. Wave propagation in layered composite laminates under periodic surface loads. *Wave Motion* **1988**, *10*, 257–266. [[CrossRef](#)]
2. Argento, A.; Scott, R. Elastic wave propagation in a Timoshenko beam spinning about its longitudinal axis. *Wave Motion* **1995**, *21*, 67–74. [[CrossRef](#)]
3. Eslami, M.; Shariyat, M.; Shakeri, M. Layerwise theory for dynamic buckling and postbuckling of laminated composite cylindrical shells. *AIAA J.* **1998**, *36*, 1874–1882. [[CrossRef](#)]
4. Eslami, M.; Javaheri, R. Buckling of composite cylindrical shells under mechanical and thermal loads. *J. Therm. Stresses* **1999**, *22*, 527–545.
5. Aghdam, M.; Falahatgar, S. Bending analysis of thick laminated plates using extended Kantorovich method. *Compos. Struct.* **2003**, *62*, 279–283. [[CrossRef](#)]
6. Rajoria, H.; Jalili, N. Passive vibration damping enhancement using carbon nanotube-epoxy reinforced composites. *Compos. Sci. Technol.* **2005**, *65*, 2079–2093. [[CrossRef](#)]
7. Formica, G.; Lacarbonara, W.; Alessi, R. Vibrations of carbon nanotube-reinforced composites. *J. Sound Vib.* **2010**, *329*, 1875–1889. [[CrossRef](#)]
8. Abanoz, M.; Yaylacı, M.; Birinci, A. Contact problems between a functionally graded layer and a rigid support. *J. Struct. Eng. Appl. Mech.* **2019**, *2*, 25–35. [[CrossRef](#)]
9. Yaylacı, M.; Eyüboğlu, A.; Adıyaman, G.; Yaylacı, E.-U.; Öner, E.; Birinci, A. Assessment of different solution methods for receding contact problems in functionally graded layered mediums. *Mech. Mater.* **2021**, *154*, 103730. [[CrossRef](#)]
10. Öner, E.; Şabano, B.-Ş.; Yaylacı, E.-U.; Adıyaman, G.; Yaylacı, M.; Birinci, A. On the plane receding contact between two functionally graded layers using computational, finite element and artificial neural network methods. *J. Appl. Math. Mech. ZAMM* **2022**, *102*, e202100287. [[CrossRef](#)]
11. Han, J.-H.; Kim, Y.-J.; Karkoub, M. Wave propagation modeling of fluid-filled pipes using hybrid analytical/two-dimensional finite element method. *Wave Motion* **2014**, *51*, 1193–1208. [[CrossRef](#)]
12. Ghadiri, M.; Malekzadeh, K.; Ghasemi, F.A. Free Vibration of an Axially Preloaded Laminated Composite Beam Carrying a Spring-Mass-Damper System with a Non-Ideal Support. *Jordan J. Mech. Ind. Eng.* **2015**, *9*, 159–207.
13. Amabili, M. A new third-order shear deformation theory with non-linearities in shear for static and dynamic analysis of laminated doubly curved shells. *Compos. Struct.* **2015**, *128*, 260–273. [[CrossRef](#)]
14. Nguyen, N.-D.; Nguyen, T.-K.; Nguyen, T.-N.; Thai, H.T. New Ritz-solution shape functions for analysis of thermo-mechanical buckling and vibration of laminated composite beams. *Compos. Struct.* **2018**, *184*, 452–460. [[CrossRef](#)]
15. Heydarpour, Y.; Aghdam, M.; Malekzadeh, P. Free vibration analysis of rotating functionally graded carbon nanotube-reinforced composite truncated conical shells. *Compos. Struct.* **2014**, *117*, 187–200. [[CrossRef](#)]
16. Zhang, L.; Lei, Z.; Liew, K. Free vibration analysis of functionally graded carbon nanotube-reinforced composite triangular plates using the FSDT and element-free IMLS-Ritz method. *Compos. Struct.* **2015**, *120*, 189–199. [[CrossRef](#)]
17. Garcia-Macias, E.; Castro-Triguero, R.; Flores, E.I.S.; Friswell, M.; Gallego, R. Static and free vibration analysis of functionally graded carbon nanotube reinforced skew plates. *Compos. Struct.* **2016**, *140*, 473–490. [[CrossRef](#)]
18. Wu, H.; Yang, J.; Kitipornchai, S. Imperfection sensitivity of postbuckling behaviour of functionally graded carbon nanotube-reinforced composite beams. *Thin-Walled Struct.* **2016**, *108*, 225–233. [[CrossRef](#)]
19. Ansari, R.; Torabi, J.; Shakouri, A.H. Vibration analysis of functionally graded carbon nanotube-reinforced composite elliptical plates using a numerical strategy. *Aerosp. Sci. Technol.* **2017**, *60*, 152–161. [[CrossRef](#)]
20. Shi, Z.; Yao, X.; Pang, F.; Wang, Q. An exact solution for the free-vibration analysis of functionally graded carbon-nanotube-reinforced composite beams with arbitrary boundary conditions. *Sci. Rep.* **2017**, *7*, 1–18.
21. Safarpour, H.; Mohammadi, K.; Ghadiri, M.; Barooti, M.M. Effect of porosity on flexural vibration of CNT-reinforced cylindrical shells in thermal environment using GDQM. *Int. J. Struct. Stab. Dyn.* **2018**, *18*, 1850123. [[CrossRef](#)]
22. Ebrahimi, F.; Seyfi, A.; Dabbagh, A. Wave dispersion characteristics of agglomerated multi-scale hybrid nanocomposite beams. *J. Strain Anal. Eng. Design.* **2019**, *54*, 276–289. [[CrossRef](#)]
23. Ebrahimi, F.; Seyfi, A. Wave propagation response of multi-scale hybrid nanocomposite shell by considering aggregation effect of CNTs. *Mech. Based Des. Struct. Mach.* **2019**, *49*, 59–80.
24. Ebrahimi, F.; Seyfi, A. Wave propagation response of agglomerated multi-scale hybrid nanocomposite plates. *Waves Random Complex Media.* **2020**, 1–25. [[CrossRef](#)]
25. Qaderi, S.; Ebrahimi, F.; Seyfi, A. An investigation of the vibration of multi-layer composite beams reinforced by graphene platelets resting on two parameter viscoelastic foundation. *SN Appl. Sci.* **2019**, *1*, 399. [[CrossRef](#)]
26. Ebrahimi, F.; Seyfi, A.; Dabbagh, A.; Tornabene, F. Wave dispersion characteristics of porous graphene platelet-reinforced composite shells. *Struct. Eng. Mech.* **2019**, *71*, 99–107.
27. Javani, M.; Kiani, Y.; Eslami, M. Thermal buckling of FG graphene platelet reinforced composite annular sector plates. *Thin-Walled Struct.* **2020**, *148*, 106589. [[CrossRef](#)]
28. Khaniki, H.B.; Ghayesh, M.H. On the dynamics of axially functionally graded CNT strengthened deformable beams. *Eur. Phys. J. Plus.* **2020**, *135*, 415. [[CrossRef](#)]

29. Trang, L.T.N.; Tung, H.V. Thermally induced postbuckling of higher order shear deformable CNT-reinforced composite flat and cylindrical panels resting on elastic foundations with elastically restrained edges. *Mech. Based Des. Struct. Mach.* **2020**, *1*–24. [[CrossRef](#)]
30. Ebrahimi, F.; Nouraei, M.; Seyfi, A. Wave dispersion characteristics of thermally excited graphene oxide powder-reinforced nanocomposite plates. *Waves Random Complex Media* **2020**, *32*, 204–232. [[CrossRef](#)]
31. Merzouki, T.; Ahmed, H.M.S.; Bessaim, A.; Haboussi, M.; Dimitri, R.; Tornabene, F. Bending analysis of functionally graded porous nanocomposite beams based on a non-local strain gradient theory. *Math. Mech. Solids*. **2022**, *27*, 66–69. [[CrossRef](#)]
32. Mahmure, A.; Tornabene, F.; Dimitri, R.; Kuruoglu, N. Free vibration of thin-walled composite shell structures reinforced with uniform and linear carbon nanotubes: Effect of the elastic foundation and nonlinearity. *Nanomaterials* **2021**, *11*, 2090. [[CrossRef](#)]
33. Ebrahimi, F.; Seyfi, A. Wave dispersion analysis of embedded MWCNTs-reinforced nanocomposite beams by considering waviness and agglomeration factors. *Waves Random Complex Media*. **2021**, 1–20. [[CrossRef](#)]
34. Lin, F.; Xiang, Y. Vibration of carbon nanotube reinforced composite beams based on the first and third order beam theories. *Appl. Math. Model.* **2014**, *38*, 3741–3754. [[CrossRef](#)]
35. Truesdell, C. *Linear Theories of Elasticity and Thermoelasticity: Linear and Nonlinear Theories of Rods, Plates, and Shells*; Springer: Berlin/Heidelberg, Germany, 2013; Volume 2.
36. Hashmi, S. *Comprehensive Materials Processing*; Newnes: Oxford, UK, 2014.
37. Ebrahimi, F.; Barati, M.R. Longitudinal varying elastic foundation effects on vibration behavior of axially graded nanobeams via nonlocal strain gradient elasticity theory. *Mech. Adv. Mater. Struct.* **2018**, *25*, 953–963. [[CrossRef](#)]
38. Loy, C.; Lam, K.; Reddy, J. Vibration of functionally graded cylindrical shells. *Int. J. Mech. Sci.* **1999**, *41*, 309–324. [[CrossRef](#)]